BAP1 loss impairs Non-Homologous End Joining DNA repair promoting genomic instability

Sabrina Caporali[1], Carla Schuy[1], Melanie Rall-Scharpf[2], Alessio Butera[1], Lisa Wiesmüller[2] and Ivano Amelio[1,]*

1. Division for Systems Toxicology, Department of Biology, University of Konstanz, Konstanz, Germany
2. Division of Gynecological Oncology, Department of Obstetrics and Gynecology, Ulm University, Ulm, Germany

*Corresponding Author:
Ivano Amelio, Chair for Systems Toxicology,
University of Konstanz, Konstanz, Germany.
Email: ivano.amelio@uni-konstanz.de

Abstract
The tumor suppressor BRCA1-associated protein 1 (BAP1) is frequently mutated in uveal melanoma, where its loss is associated with poor prognosis and metastatic progression. Although BAP1 is known to regulate homologous recombination (HR), its role in non-homologous end-joining (NHEJ) has remained unexplored. Here, we show that BAP1 functions as a central regulator of DNA double-strand break (DSB) repair, controlling both HR and NHEJ to preserve genomic integrity. BAP1 depletion in uveal melanoma cells impairs recruitment of RAD51 and 53BP1, thereby disrupting HR and NHEJ, respectively. Mechanistically, this dual defect is driven by aberrant accumulation of H2AK119ub at DSB sites, which inappropriately promotes DNA end resection. In G1-phase cells, this unscheduled resection inhibits NHEJ, the normally dominant repair mechanism in this phase. Pharmacological inhibition of H2AK119 ubiquitylation using PTC-209 restores 53BP1 localization and suppresses aberrant resection, establishing a causal link between BAP1-regulated chromatin dynamics and DSB repair pathway choice. Clinically, BAP1 loss correlates with pronounced genomic instability, providing a mechanistic explanation for its association with poor outcomes in uveal melanoma. Collectively, these findings identify BAP1 as a gatekeeper of DSB repair fidelity, safeguarding NHEJ in G1 and HR in S/G2, and highlight H2AK119ub modulation as a potential therapeutic strategy to target vulnerabilities in BAP1-deficient tumors. This work reveals a previously unrecognized role for BAP1 in safeguarding NHEJ activation. BAP1 loss derails repair pathway balance, fueling genome instability and driving uveal melanoma progression.

Introduction
The ability of cells to sense and repair DNA double-strand breaks (DSBs), induced by endogenous or exogenous stressors such as chemotherapeutic agents or environmental insults, is essential for maintaining genome integrity[1]. These highly toxic lesions interfere with vital processes including DNA replication and transcription, and, if left unrepaired or misrepaired, can lead to genomic alterations that profoundly affect cellular behavior [2]. The accurate execution and proper choice between the two main DSB repair pathways, non-homologous end-joining (NHEJ) and homologous recombination (HR), are tightly regulated by histone post-translational modifications[3]. These modifications dynamically remodel chromatin to recruit the appropriate repair factors to DNA damage sites [4,5]. For example, ubiquitilation of Histone H4 at lysine 20 (H4K20me2) and Histone H2A at lysine 15 (H2AK15ub) at DSB-flanking nucleosomes promote 53BP1 recruitment and downstream effectors that suppress DNA-end resection, thereby facilitating NHEJ [6]. Conversely, ubiquitylation of Histone H2A at lysine 127 (H2AK127 by) the BRCA1/BARD1 E3 ligase complex promotes HR [7]. Intriguingly, monoubiquitylation of Histone H2A at lysine 119 (H2AK119ub) has also emerged as a regulator of repair pathway choice: Polycome Repressive Complex 1 (PRC1)-mediated H2AK119ub deposition at DSBs support recruitment of the resection factor CtIP, thereby initiating end resection and promoting HR [8].

The tumor suppressor BRCA1-associated protein 1 (BAP1) is a nuclear ubiquitin carboxy-

terminal hydrolase (UCH) that functions as the catalytic subunit of the Polycomb repressive deubiquitinase (PR-DUB) complex [9,10]. By removing H2AK119ub deposited by PRC1, BAP1 counteracts PRC1 activity, thereby reshaping chromatin landscapes, transcriptional programs, and key cellular processes including cell cycle progression, metabolism and cell death [11]. BAP1 has been implicated in the DNA damage response: it is phosphorylated by ATM upon DNA damage and localizes to break sites. BAP1-deficient cells display impaired HR and defective DSB repair [12,13]. However, the potential role of BAP1 in regulating NHEJ activation and execution has remained unexplored.

BAP1-associated tumorigenesis shows a distinctive spectrum, with a high frequency of mutations in relatively rare cancers such as uveal melanoma and malignant mesothelioma [11,14]. Uveal melanoma is the most common primary intraocular malignancy in adults, characterized by high lethality due to its propensity to metastasize, most often to the liver. Approximately 50% of patients develop metastases, with a median survival of ~12 months following diagnosis [15]. While radiotherapy and enucleation can control primary tumors, no effective systemic therapies exist for metastatic uveal melanoma [16]. BAP1 mutations are frequent in uveal melanoma, and its inactivation strongly correlates with metastatic dissemination and poor prognosis [17,18]. Understanding the molecular mechanisms by which BAP1 loss promotes tumor progression and therapy resistance in UM is therefore of urgent clinical importance.

In this study, we demonstrate that BAP1 loss drives pronounced genomic instability in uveal melanoma. Mechanistically, we show that BAP1 deficiency impairs not only HR but also NHEJ, rendering cells unable to efficiently repair DSBs. In particular, BAP1 depletion induces aberrant DNA end resection in G1-phase cells, thereby antagonizing NHEJ. These findings establish BAP1 as a central regulator of DSB repair pathway choice and, importantly, reveal for the first time a mechanistic link between BAP1 activity and NHEJ regulation, with direct implications for genomic stability and therapeutic vulnerabilities in uveal melanoma.

Results

BAP1 mutations predict poor prognosis in uveal melanoma

The BAP1 gene locus is predominantly altered in specific tumors associated with the BAP1 tumor predisposition syndrome, including uveal melanoma, mesothelioma, intrahepatic cholangiocarcinoma (ICC), and kidney renal clear cell carcinoma (ccRCC), with alteration frequencies of approximately 36%, 36%, 19%, and 10%, respectively, compared with only ~3% across all human cancers (**Figure 1A**). In uveal melanoma, patients carrying BAP1 mutations exhibit significantly reduced overall survival (**Figure 1B**), shorter disease-free survival (**Figure 1C**), and a greater prevalence of additional adverse prognostic markers (**Figure 1D**). Interestingly, this prognostic effect was not observed in individuals with malignant mesothelioma (**Supplemental Figure S1A**).

BAP1 has been broadly implicated in maintaining genome integrity, in part through its role in HR–mediated repair of DSBs. We therefore investigated whether BAP1 mutational status correlates with genomic instability. In uveal melanoma, BAP1-mutated tumors displayed significantly higher levels of aneuploidy, fraction of the genome altered, and microsatellite instability (MSI) scores, compared with wild-type tumors (**Figure 1E**). This association, however, was not evident in other tumor types characterized by frequent BAP1 alterations (**Supplemental Figure S1B, S1C, S1D**). Together, these findings suggest that BAP1 mutations drive distinct mechanisms of genomic instability in uveal melanoma, which may underlie the prognostic impact of BAP1 mutations.

BAP1 loss compromises DSB repair in uveal melanoma cells

We next investigated the molecular mechanisms underlying the compromised genome integrity observed in uveal melanocytes upon loss of BAP1. For this purpose, we used the BAP1-proficient human uveal melanoma cell line MP41. Because stable CRISPR/Cas9-mediated deletion of BAP1 was incompatible with *in vitro* survival of these cells, we reduced BAP1 expression using two independent short interfering RNAs (siRNAs). As expected, BAP1 depletion led to the

accumulation of the H2AK119ub histone mark, a well-established post-translational modification dynamically regulated by BAP1 deubiquitinase activity (**Figure 1F**) [19].

We next evaluated the impact of BAP1 loss on the resolution kinetics of DSBs following genotoxic stress. BAP1-deficient cells displayed impaired clearance of bleomycin-induced DNA damage over time (**Figure 1G**). In agreement, immunofluorescence staining for γH2A.X showed an increased proportion of pan-nuclear γH2A.X$^+$ cells during the early time point of recovery (0 and 1h) after 24h bleomacyn in BAP1-silenced cells compared with controls (**Figure 1H,I and Supplemental Figure S1E**). Together, these results demonstrate that BAP1 loss impairs DSB repair capacity, thereby compromising the maintenance of genome stability.

To further dissect the mechanistic role of BAP1 in double-strand break (DSB) repair in uveal melanoma, we examined the recruitment of key upstream repair factors from both the homologous recombination (HR) and non-homologous end joining (NHEJ) pathways following DSB induction. As anticipated from prior studies [12,13], BAP1-depleted cells exhibited a pronounced defect in RAD51 foci formation compared with BAP1-proficient cells, both immediately after bleomycin removal and early stage recovery (0 and 1h) (**Figure 2A-C**). Consistent with this, RAD51 was efficiently recruited to damage sites at 3 h post-ionizing radiation (IR) in control MP41 cells, but failed to accumulate in both BAP1- and BRCA1-depleted cells **(Supplemental Figures S2A–S2D**).

We next analyzed the recruitment of 53BP1, a critical regulator of DSB repair pathway choice that inhibits DNA end-resection and promotes NHEJ in G1 cells [4]. Unexpectedly, BAP1-depleted cells displayed also a drastic reduction in 53BP1 foci formation across all recovery time points (0 h, 1 h, and 2 h) following 24 h bleomycin treatment (**Figure 2D-F**). To strenghten and generalise these findings we also tested the response of BAP1-deficient cells under IR treatment, where they failed to engage 53BP1 loading at the damage site 1-3h post IR (**Supplemental Figures S2E, S2F, S2G**).

Together, these results indicate that BAP1 loss impairs the recruitment of both RAD51 and 53BP1 to DSBs, thereby disrupting key steps of both HR and NHEJ repair pathways**.**

BAP1 is required for execution of both HR and NHEJ DNA repair pathways

Based on the observation that markers of both HR and NHEJ were altered upon BAP1 silencing, we next sought to determine whether this was the result of a correlative observation or of a specific impact of BAP1 on the execution of these DSB repair pathways.

To this end, we employed stably integrated reporter plasmids that allow quantification of HR and NHEJ activity. Specifically, we used the HR-EGFP/5′EGFP (**Figure 3A**) and HR-EGFP/3′EGFP (**Supplemental Figure S3A**) reporters to monitor HR [20], along with the PIMEJ5GFP reporter system to assess NHEJ (**Supplemental Figure 3A**)[21]. Notably, the HR-EGFP/5′EGFP reporter detects exclusively conservative HR, whereas the HR-EGFP/3′EGFP reporter captures both conservative HR and single-strand annealing (SSA). Both HR reporters contain a mutated EGFP gene harboring an I-SceI restriction site, along with either a 3′EGFP or 5′EGFP donor sequence in tandem, which serves as a template for repair by HR. In contrast, the PIMEJ5GFP reporter contains two distal tandem I-SceI recognition sites flanking both a puromycin resistance cassette and the EGFP gene. Expression of I-SceI and its subsequent nuclear translocation induces site-specific DSBs within the reporters. Restoration of EGFP fluorescence occurs only when the break is successfully repaired, via HR in the HR reporters (HR-EGFP/5′EGFP or HR-EGFP/3′EGFP), or via NHEJ in the PIMEJ5GFP system.

Analysis of HR-EGFP/5′EGFP cells showed that repair capacity (RFP$^+$GFP$^+$ population) was markedly reduced to 26.5% upon BAP1 depletion (**Figure 3B,C; Supplemental Figures S4A, S4C**). A similar reduction was observed in the HR-EGFP/3′EGFP clone (**Supplemental Figures S3B-D**). Remarkably however, we also found that NHEJ repair efficiency decreased to 58% in siBAP1-depleted cells (**Figures 3E,F; Supplemental Figures S4B, S4D**), consistent with the defective 53BP1 localization of BAP1 deficient cells. Together, these results indicate that BAP1 loss impairs not only HR but also the NHEJ double-strand break repair pathway.

BAP1 loss triggers aberrant DNA end resection in G1

The ubiquitination of histone H2A at lysine 119 (H2A-K119ub) at DSB sites regulates DNA end resection and consequently the execution of HR[8]. As BAP1 is responsible for removing H2A-

K119ub, we hypothesized that BAP1 loss might underlie aberrant DNA end resection in uveal melanoma cells following DSB induction across different cell cycle phases. Consistent with this hypothesis, BAP1 depletion caused an accumulation of H2A-K119ub in G1 cells untreated and exposed to X-ray (**Figure 4A, Supplemental S5A**). To formally prove this, we analyzed RPA recruitment, a marker of DNA end resection, upon DNA damage. BAP1 depletion led to an increase in total RPA foci formation during DSB recovery (**Figure 4B,C, Supplemental S5B**), indicating a general aberrant control of DNA end resection. To determine the cell cycle specificity of this effect, we examined RPA foci formation in Cyclin A2–positive (S/G2) and Cyclin A2–negative (G1) cells in both BAP1-proficient and -deficient backgrounds. This analysis revealed that BAP1 loss did not alter RPA recruitment in G2 cells (Cyclin $A2^{+}$) (**Figure 4D and F**), consistent with normal end resection during this phase that preferentially favours activation of HR. However in contrast, G1 cells (Cyclin $A2^{-}$) exhibited a substantial accumulation of RPA foci upon BAP1 depletion (**Figure 4E and F**), indicating activation of unscheduled DNA end resection in G1. Together, these data demonstrate that BAP1 loss triggers unscheduled DNA end resection and RPA recruitment in G1 cells, which likely prevents NHEJ activation and impairs resolution of DSBs.

H2AK119ub accumulation in BAP1-depleted cells counteracts NHEJ by promoting DNA end resection

To establish a causal link between BAP1 loss, H2AK119ub accumulation, and aberrant DSB repair pathway choice in G1 cells, we treated uveal melanoma cells with PTC-209, a small-molecule inhibitor that reduces H2AK119 ubiquitylation by targeting BMI-1, the catalytic subunit of the PRC1 complex [22]. Cell cycle–resolved analysis of RPA recruitment showed that inhibition of H2AK119ub accumulation by PTC-209, three hours post-irradiation, reduced RPA loading in G1-phase (Cyclin A2–negative) cells (**Figure 5A-C, Supplemental S5C,D**). This suggests that aberrant DNA end resection contributes to defective NHEJ activation in BAP1-depleted G1 cells. To test whether PTC-209 could reverse the reduction of 53BP1 accumulation in BAP1-deficient cells after irradiation, we measured 53BP1 recruitment. As predicted, PTC-209 restored 53BP1 loading (**Figure 5D,E**), establishing a causal relationship between H2AK119ub accumulation in BAP1-deficient G1 cells, aberrant end resection (RPA recruitment), and impaired NHEJ (**Figure 5F**).

Together, these findings highlight that BAP1-mediated deubiquitylation of H2AK119ub is essential for proper engagement of NHEJ in G1 cells and for maintaining correct DSB repair pathway choice.

Discussion

Our study uncovers a previously unrecognized role for BAP1 in regulating the execution of NHEJ DSB repair, with direct implications for the genomic instability and aggressive clinical behavior of uveal melanoma. While BAP1 has been linked to HR through earlier reports [12,13], our findings establish that its function extends beyond HR, encompassing a crucial role in NHEJ. Specifically, we show that BAP1 loss triggers aberrant DNA end resection in G1 cells, thereby antagonizing NHEJ and leaving cells unable to effectively resolve DSBs. This dual impairment of both HR and NHEJ provides a mechanistic explanation for the pronounced genomic instability associated with BAP1 mutations in uveal melanoma (**Figure 5F**).

Histone post-translational modifications are well-established regulators of DSB pathway choice, acting as dynamic chromatin signals that guide the recruitment of repair factors [5]. Our work highlights the importance of H2AK119 ubiquitylation as a determinant of pathway engagement. We demonstrate that, in the absence of BAP1, accumulation of H2AK119ub at DSB sites drives unscheduled recruitment of the resection factor RPA in G1-phase cells. This inappropriate activation of end resection prevents 53BP1 loading, thus impairing NHEJ, a repair pathway canonically required during G1 when homologous templates are unavailable. Importantly, pharmacological inhibition of H2AK119ub deposition with PTC-209 restored 53BP1 accumulation and reduced aberrant resection, establishing a direct causal link between BAP1-regulated deubiquitylation, chromatin remodelling at DSBs, and pathway choice.

These findings place BAP1 alongside other chromatin regulators that govern DSB repair pathway fidelity. BAP1 safeguards NHEJ in G1 by preventing inappropriate resection. Thus, BAP1

functions as a central “gatekeeper” of pathway choice, ensuring that DSBs are repaired by the correct mechanism according to cell cycle context. The simultaneous impairment of HR and NHEJ in BAP1-deficient cells creates a unique state of “repair exhaustion,” which may drive the accumulation of structural alterations and aneuploidy observed in BAP1-mutated uveal melanoma tumors.

From a clinical perspective, these insights provide a mechanistic basis for the aggressive phenotype and poor prognosis of BAP1-mutant uveal melanoma. They also suggest potential therapeutic vulnerabilities. On one hand, defective HR renders these tumors potentially sensitive to PARP inhibitors or other agents that exploit HR deficiency. On the other hand, the unexpected impairment of NHEJ may influence responses to radiotherapy or genotoxic chemotherapy, as cells lacking both major repair pathways might accumulate lethal damage but could also activate compensatory error-prone mechanisms. Targeting H2AK119ub dynamics, as demonstrated with BMI1 inhibition, may represent a novel therapeutic strategy to restore repair pathway balance or exploit vulnerabilities specific to BAP1-deficient cancers.

In summary, our work identifies BAP1 as a critical regulator of DSB repair pathway choice. By restraining H2AK119ub-driven end resection in G1 cells, BAP1 ensures proper engagement of NHEJ, thereby maintaining genomic stability. Loss of this regulation simultaneously disables HR and NHEJ, fuelling genome instability and tumour progression in uveal melanoma. These findings not only advance the understanding of BAP1 biology but also open new avenues for therapeutic intervention in BAP1-deficient tumours.

Funding. This work has been supported by the DFG to IA, (under the TRR353 “Death Decision” projects A05), the Carl Zeiss Stiftung to IA (Endowed Professorship, #15972218, 2022-2027; Prisma Programme, #P2022-5-003), by the cooperation between Carl Zeiss Stiftung and German Scholars Organization with the Fund for international researchers to IA (#15978021).

Data Availability. All the data are made available upon request.

Materials availability

All unique/stable reagents generated in this study are available from the lead contact with a completed materials transfer agreement.

Authors Contribution

Conceptualization, IA; methodology, SC, MRS; investigation, SC, CS, AB and MRS; writing – original draft, SC; writing – review & editing, LW and IAl resources, LW and IA; supervision, LW and IA

Declarations of interests

The Authors declare that they have no competing interests.

Material and Methods

Cell culture and siRNA transfection

MP41 human cells were purchased from ATCC (MP41-CRL-3297 ™) and were maintained in RPMI medium (Gibco) supplemented with 20% fetal bovine serum (FBS), sodium pyruvate (1 mM), Hepes Buffer (10 mM) and penicillin–streptomycin (100 U/ml).

U2OS human cells were purchased from ATCC (HTB-96 ™ATCC) and were maintained in Dulbecco's Modified Eagle Medium (DMEM) supplemented with 10% FBS and penicillin-streptomycin (100 U/ml). All cell lines were grown at 37°C, 5% CO2.

For silencing experiments cells were transfected with 20 nM of scramble (siCTRL) or BAP1 (s15821, s15822, ThermoFisher Scientific) or BRCA1 (S459, Thermofisher Scientific) targeting siRNAs using Lipofectamine RNAiMAX (Invitrogen, ThermoFisher Scientific) according to the manufacturer's protocol. All cell lines were collected at 72 hours from siRNA transfection. For DNA damage experiments, MP41 siCTRL or siBAP1-transfected cells were treated with bleomycin (50 µg/ml) for 24 hours or irradiated with 5 Gy. For RPA and 53BP1 immunofluorescence experiments, BAP1-depleted MP41 cells were treated with DMSO or 0,1 µM PTC-209 (BMI-inhibitor, Sigma Aldrich) for 48 hours prior IR-induced DNA damage. Cells were then collected for immunofluorescence or western blot analysis at the indicated hours post drug removal or IR-induced DSBs.

Generation of stable cell lines with integrated reporters

For the generation of U2OS clones with stably chromosomally integrated DSB repair reporters, U2OS cells were transfected with 5 µg of the following plasmids, Pim-EJ5-GFP (Addgene, Plasmid #44026)[21], HR-EGFP/3'EGFP or HR-EGFP/5'EGFP [20] using PEI reagent according to the manufacturers' instructions.

U2OS transfected cells were maintained in complete RPMI medium supplemented with 2 µM of Puromycin. After Puromycin selection, isolation of individual cell clones for each repair plasmid were obtained by serial dilution. Single clones were then amplified and tested for EGFP fluorescence upon I-SCEI induction using flow cytometry (Beckman Coulter CytoFLEX™).

DNA Damage Reporter Assays

HR-EGFP/3'EGFP, HR-EGFP/5'EGFP and Pim-EJ5-GFP U2OS clones were transfected with siRNA control or against BAP1 (s15822) or BRCA1 to assess repair efficiency respectively of homologous recombination (HR) and single-strand annealing (SSA), conservative HR (cHR) and total non-homologous end joining (NHEJ) DNA repair pathways.

All U2OS clones were transfected with 2 µg I-SceI-RFP plasmid (Addgene, #17654)[21] and after 24 hours, treated with 0.4 µM triamcinolone acetonide (TCA) or DMSO. TCA-driven-I-SceI-RFP nuclear translocation led to a site-specific cleavage within the integrated EGFP DNA sequence. DNA repair efficiency for HR or NHEJ was evaluated by measuring the EGFP fluorescence signal upon the reconstitution of the functional EGFP coding sequence.

As a positive control for EGFP fluorescence, U2OS cells were co-transfected with wtEGFP [20] and I- SceI -RFP plasmids as described previously. Sample were collected at 72 h post-silencing and 24 h post-TCA induction. EGFP and RFP fluorescence signals were detected by flow cytometric analysis using the Beckman Coulter CytoFLEX™ and at least 10000 events were acquired for each condition. The percentage of Individual GFP-positive cells were then examined within the RFP-positive cell population.

Protein Extraction and Western blot analysis

MP41 or U2OS cells were lysed using RIPA buffer supplemented with protease and phosphatase inhibitors (Sigma Aldrich). 20 µg of proteins were then denatured at 98°C for 10 minutes, resolved on a SDS–polyacrylamide gel and transferred onto an Amersham Hybond P0.45 PVDF membrane (Sigma Aldrich). Membranes were incubated with a blocking solution of 5% non-fat dried milk diluted in PBS 0.1% Tween-20 for 2h at RT.

The following primary antibodies were incubated overnight at 4°C: rabbit BAP1 (D7W70) mAB (Cell Signaling Technology, 13271S), mouse Anti-β-Actin (Sigma Aldrich, A1978-200UL), mouse BRCA1 (D-9) monoclonal IgG (Santa Cruz Biotechnology, sc-6954), mouse monoclonal anti-GAPDH, clone GAPDH-71.1 (Sigma Aldrich, G8795-200UL), mouse Anti-phospho-Histone H2A.X (Ser139), clone JBW301 (Merck/Sigma, 05-636-I), rabbit H3 (D1H2) mAb (Cell Signaling, # 4499), Ubiquityl-Histone H2A (Lys119) (D27C4) XP® Rabbit mAb (Cell Signaling, #8240) and anti-Histone H2A (Abcam, ab18255). Membrane were then incubated with the appropriate anti- mouse or anti- rabbit peroxidase-conjugated secondary antibodies (Bio-Rad) at room temperature for 1 h. Chemiluminescence signals were detected using ECL chemiluminescence kit (Thermofisher , #32106X4) or SuperSignalTM West Dura Extended Duration Substrate (Thermofisher).

RNA extraction, RT and qPCR

RNA extraction was performed using RNeasy Mini Kit (Qiagen) according to the manufacturer's instruction. 1 µg of extracted RNA was successively reverse transcribed with the SensiFAST cDNA Synthesis kit (Biocat, BIO-65054). Real time PCR (qPCR) was performed using PerfeCTa® SYBR® Green FastMix (VWR, 733-1390). For the amplification of target genes, the following primers were used: hBAP1 Fw 5'- CGGGTCATCATGGAGCGTAT -3', hBAP1 Rev 5'- ACCACTGCCATCAGGTTGAA -3', hTBP Fw 5'- TCAAACCCAGAATTGTTCTCCTTAT -3', hTBP Rev 5'- CCTGAATCCCTTTAGAATAGGTAGA -3'. qPRC results were expressed as a relative gene expression and calculated following the $2^{-\Delta\Delta ct}$ method after normalization to human TATA-binding protein (TBP) using QuantStudio qPCR System (ThermoFIscher).

Immunofluorescence

MP41 cells were seeded on circular glass slides and treated with bleomycin or irradiated as reported before. Samples were fixed in Paraformaldehyde (PFA) 4% in PBS (phosphate-buffered saline) for 15 minutes at RT and permeabilized with 0.01% Triton™ X-100 (Sigma, #T8787) for 10 minutes at RT. Blocking was performed with 2% Bovine Serum Albumin (BSA) in PBS 1x for 2h at RT and slides were then incubated with the following primary antibodies overnight at 4°C: mouse Anti-phospho-Histone H2A.X (Ser139), clone JBW301 (Merck/Sigma, 05-636-I), rabbit Anti-RAD51 [EPR4030(3)] (Abcam, ab133534) mouse Anti-RPA32/RPA2 antibody (Abcam, ab2175) rabbit Anti-53BP1 IgG (Abcam, ab36823) rabbit Cyclin A2 (E6D1J) mAb (Cell Signaling, # 67955). After 3 washes with PBS 1x, slides were incubated with anti-mouse or anti-rabbit Alexa Fluor secondary antibody (Invitrogen) and DAPI (Sigma Aldrich) to counterstain nuclei for 1h at RT. Following 3 washes with PBS 1x, samples were mounted with ProLong™ Gold Antifade mountant (Invitrogen #P36934) and acquired using z-stack mode with a point laser scanning confocal microscope (Zeiss LSM 700, ZEN software). All the acquired images were processed using FIJI software (ImageJ).

Bioinformatic analyses

Data about patients for human uveal melanoma, pleural mesothelioma, Intrahepatic Cholangiocarcinoma and Kidney Renal Clear Cell Carcinoma were retrieved by cBioportal database (http://www.cbioportal.org). Patient cohort for all the analyzed datasets was divided in two group according BAP1 mutation status (WT vs Mut).

Statistical analyses

All graphs and statistical analyses were performed using GraphPad Prism 9.0 (GraphPad Software Inc.). All results are expressed as median or mean (where indicated). Statistical analysis for data retrieved from cBioportal databases was performed by using unpaired t-test while for immunofluorescence data by Ordinary one-way ANOVA, Tukey's correction. For Kaplan–Meier analysis, the Mantel-Cox test was applied. All experiments were performed with at least three biological replicates excluding where reported.

References

1. Ceccaldi, R., Rondinelli, B., and D'Andrea, A.D. (2016). Repair Pathway Choices and Consequences at the Double-Strand Break. Trends Cell Biol *26*, 52-64. 10.1016/j.tcb.2015.07.009.
2. Jackson, S.P., and Bartek, J. (2009). The DNA-damage response in human biology and disease. Nature *461*, 1071-1078. 10.1038/nature08467.
3. Ceccaldi, R., and Cejka, P. (2025). Mechanisms and regulation of DNA end resection in the maintenance of genome stability. Nat Rev Mol Cell Biol *26*, 586-599. 10.1038/s41580-025-00841-4.
4. Cejka, P., and Symington, L.S. (2021). DNA End Resection: Mechanism and Control. Annu Rev Genet *55*, 285-307. 10.1146/annurev-genet-071719-020312.
5. Clouaire, T., and Legube, G. (2019). A Snapshot on the Cis Chromatin Response to DNA Double-Strand Breaks. Trends Genet *35*, 330-345. 10.1016/j.tig.2019.02.003.
6. Fradet-Turcotte, A., Canny, M.D., Escribano-Diaz, C., Orthwein, A., Leung, C.C., Huang, H., Landry, M.C., Kitevski-LeBlanc, J., Noordermeer, S.M., Sicheri, F., and Durocher, D. (2013). 53BP1 is a reader of the DNA-damage-induced H2A Lys 15 ubiquitin mark. Nature *499*, 50-54. 10.1038/nature12318.
7. Densham, R.M., Garvin, A.J., Stone, H.R., Strachan, J., Baldock, R.A., Daza-Martin, M., Fletcher, A., Blair-Reid, S., Beesley, J., Johal, B., et al. (2016). Human BRCA1-BARD1 ubiquitin ligase activity counteracts chromatin barriers to DNA resection. Nat Struct Mol Biol *23*, 647-655. 10.1038/nsmb.3236.
8. Fitieh, A., Locke, A.J., Mashayekhi, F., Khaliqdina, F., Sharma, A.K., and Ismail, I.H. (2022). BMI-1 regulates DNA end resection and homologous recombination repair. Cell Rep *38*, 110536. 10.1016/j.celrep.2022.110536.
9. Masclef, L., Ahmed, O., Estavoyer, B., Larrivee, B., Labrecque, N., Nijnik, A., and Affar, E.B. (2021). Roles and mechanisms of BAP1 deubiquitinase in tumor suppression. Cell Death Differ *28*, 606-625. 10.1038/s41418-020-00709-4.
10. Conway, E., Rossi, F., Fernandez-Perez, D., Ponzo, E., Ferrari, K.J., Zanotti, M., Manganaro, D., Rodighiero, S., Tamburri, S., and Pasini, D. (2021). BAP1 enhances Polycomb repression by counteracting widespread H2AK119ub1 deposition and chromatin condensation. Mol Cell *81*, 3526-3541 e3528. 10.1016/j.molcel.2021.06.020.
11. Carbone, M., Harbour, J.W., Brugarolas, J., Bononi, A., Pagano, I., Dey, A., Krausz, T., Pass, H.I., Yang, H., and Gaudino, G. (2020). Biological Mechanisms and Clinical Significance of BAP1 Mutations in Human Cancer. Cancer Discov *10*, 1103-1120. 10.1158/2159-8290.CD-19-1220.
12. Yu, H., Pak, H., Hammond-Martel, I., Ghram, M., Rodrigue, A., Daou, S., Barbour, H., Corbeil, L., Hebert, J., Drobetsky, E., et al. (2014). Tumor suppressor and deubiquitinase BAP1 promotes DNA double-strand break repair. Proc Natl Acad Sci U S A *111*, 285-290. 10.1073/pnas.1309085110.
13. Ismail, I.H., Davidson, R., Gagne, J.P., Xu, Z.Z., Poirier, G.G., and Hendzel, M.J. (2014). Germline mutations in BAP1 impair its function in DNA double-strand break repair. Cancer Res *74*, 4282-4294. 10.1158/0008-5472.CAN-13-3109.
14. He, M., Chaurushiya, M.S., Webster, J.D., Kummerfeld, S., Reja, R., Chaudhuri, S., Chen, Y.J., Modrusan, Z., Haley, B., Dugger, D.L., et al. (2019). Intrinsic apoptosis shapes the tumor spectrum linked to inactivation of the deubiquitinase BAP1. Science *364*, 283-285. 10.1126/science.aav4902.

15. Krantz, B.A., Dave, N., Komatsubara, K.M., Marr, B.P., and Carvajal, R.D. (2017). Uveal melanoma: epidemiology, etiology, and treatment of primary disease. Clin Ophthalmol *11*, 279-289. 10.2147/OPTH.S89591.
16. Chua, V., Mattei, J., Han, A., Johnston, L., LiPira, K., Selig, S.M., Carvajal, R.D., Aplin, A.E., and Patel, S.P. (2021). The Latest on Uveal Melanoma Research and Clinical Trials: Updates from the Cure Ocular Melanoma (CURE OM) Science Meeting (2019). Clin Cancer Res *27*, 28-33. 10.1158/1078-0432.CCR-20-2536.
17. Decatur, C.L., Ong, E., Garg, N., Anbunathan, H., Bowcock, A.M., Field, M.G., and Harbour, J.W. (2016). Driver Mutations in Uveal Melanoma: Associations With Gene Expression Profile and Patient Outcomes. JAMA Ophthalmol *134*, 728-733. 10.1001/jamaophthalmol.2016.0903.
18. Karlsson, J., Nilsson, L.M., Mitra, S., Alsen, S., Shelke, G.V., Sah, V.R., Forsberg, E.M.V., Stierner, U., All-Eriksson, C., Einarsdottir, B., et al. (2020). Molecular profiling of driver events in metastatic uveal melanoma. Nat Commun *11*, 1894. 10.1038/s41467-020-15606-0.
19. Szczepanski, A.P., and Wang, L. (2021). Emerging multifaceted roles of BAP1 complexes in biological processes. Cell Death Discov *7*, 20. 10.1038/s41420-021-00406-2.
20. Akyuz, N., Boehden, G.S., Susse, S., Rimek, A., Preuss, U., Scheidtmann, K.H., and Wiesmuller, L. (2002). DNA substrate dependence of p53-mediated regulation of double-strand break repair. Mol Cell Biol *22*, 6306-6317. 10.1128/MCB.22.17.6306-6317.2002.
21. Bennardo, N., Cheng, A., Huang, N., and Stark, J.M. (2008). Alternative-NHEJ is a mechanistically distinct pathway of mammalian chromosome break repair. PLoS Genet *4*, e1000110. 10.1371/journal.pgen.1000110.
22. Kreso, A., van Galen, P., Pedley, N.M., Lima-Fernandes, E., Frelin, C., Davis, T., Cao, L., Baiazitov, R., Du, W., Sydorenko, N., et al. (2014). Self-renewal as a therapeutic target in human colorectal cancer. Nat Med *20*, 29-36. 10.1038/nm.3418.

Figure legends

Figure 1. BAP1 mutations in uveal melanoma (UM) are associated with genomic instability.
(A) Frequency of BAP1 genetic alterations in tumors from the BAP1 cancer predisposition syndrome and in pan-cancer cohorts of metastatic tumors. Patient cohorts were retrieved from QIMR Oncotarget 2016 and TCGA Firehose Legacy (UM), TCGA PanCancer Atlas (mesothelioma and kidney renal clear cell carcinoma), MSK Hepatology 2021 (intrahepatic cholangiocarcinoma), and MSK Cell 2021 (pan-cancer) datasets via the cBioPortal platform. Data are shown as bar plots.
(B, C) Kaplan–Meier survival curves for overall survival (B) and disease-free survival (C) in UM patients with BAP1 wild-type (green) or BAP1-mutated (red) tumors. P-values are indicated. Data were retrieved from QIMR Oncotarget 2016 and TCGA Firehose Legacy.
(D, E) Violin plots showing tumor basal diameter, tumor thickness (D), aneuploidy score, fraction of genome altered and microsatellite instability (MSI) score (E) in BAP1 wild-type versus BAP1-mutated UM patients. Orange line: median. ***p < 0.01, *p < 0.05, ns: not significant*. P-values were calculated using an unpaired t-test.
(F) Western blot analysis of BAP1 silenced MP41 cells.
(G) Western blot analysis of γH2AX in MP41 cells following BAP1 silencing. MP41 cells were treated with bleomycin (50 µg/ml, 24 h) and collected at the indicated recovery time points.
(H, I) Representative immunofluorescence images of pan-nuclear γH2AX+ MP41 cells (red) at the indicated recovery time points after bleomycin treatment upon BAP1 silencing. DAPI stains DNA (blue) (H). Violin plot quantifying the percentage of pan-nuclear γH2AX+ cells per field across 3 independent experiments (I). Each dot represents a field. Red line: median. Scale bar: 10 µm. ****p < 0.001, **p < 0.01, *p < 0.05, ns: not significant.* P-values were determined by one-way ANOVA with Tukey's correction.

Figure 2. BAP1 depletion impairs the recruitment of HR and NHEJ repair factors.
(A) Representative confocal images of RAD51 (red) in MP41 cells transfected with siCTRL or siBAP1. DAPI stains DNA (blue). Scale bar: 10 µm.
(B, C) Scattered plots showing the number of RAD51 foci per cell (B) or violin plots showing the proportion of RAD51+ cells (>5 foci/nucleus) (C) over the total cells per field (dots) in 3 independent experiments. Red line: median. ***p < 0.001, **p < 0.01, ns: not significant. P-values by one-way ANOVA with Tukey's correction.
(D) Representative confocal images of 53BP1 (green) in MP41 cells transfected with siCTRL or siBAP1. DAPI stains DNA (blue). Scale bar: 10 µm.
(E, F) Scattered plots showing the number of 53BP1 foci per cell (E) or violin plots showing the proportion of RAD51+ cells (>5 foci/nucleus) (F) over the total cells per field (dots) in 3 independent experiments. Red line: median. ****p < 0.0001,***p < 0.001, **p < 0.01, *p < 0.05, ns: not significant. P-values by one-way ANOVA with Tukey's correction.

Figure 3. Loss of BAP1 compromises HR and NHEJ repair efficiency.
(A, D) Schematics of the HR-EGFP/5′EGFP (A) and PIMEJ5GFP (D) reporter constructs. HR-EGFP/5′EGFP includes a mutated EGFP gene containing an I-SceI recognition site and a truncated 5′EGFP sequence serving as a repair template. PIMEJ5GFP contains two distal I-SceI sites flanking a puromycin gene and the EGFP sequence. Stable U2OS clones with chromosomally integrated reporters were transfected with siCTRL, siBAP1, or siBRCA1. The following day, cells were transfected with I-SceI-RFP (red fluorescence) and treated with triamcinolone acetonide (TCA) 24 h later to induce nuclear translocation of I-SceI. RFP+ cells were analyzed for GFP fluorescence.
(B, E) Representative flow cytometry plots showing GFP+ cells (yellow gate) within the RFP+ population under each condition. GFP fluorescence: B525-FITC-A; side scatter: SSC.
(C, F) Bar plots quantifying HR (C) and NHEJ (F) repair efficiency across ≥3 independent experiments (dots). Data normalized to control and presented as mean ± SD. ****p < 0.0001. P-values by one-way ANOVA with Tukey's correction (C) or paired t-test (F).

Figure 4. BAP1 depletion promotes RPA recruitment in G1 phase.

(A) Western blot analysis of H2AK119ub levels upon BAP1 depletion in G1 cells. MP41 were irradiated (5 Gy) at 6 hours from Nocodazole release and collected 3 hours post IR

(B, C) Scatter dot plots quantifying RPA foci (green in C) during recovery from bleomycin treatment in MP41 cells depleted of BAP1. Representative immunofluorescence images are shown in B. DAPI stains DNA. Scale bar: 10 µm. Red line: mean. ****p < 0.0001, **p < 0.01, ns: not significant. P-values by one-way ANOVA with Tukey's correction
(D–F) Scatter dot plots quantifying RPA foci in Cyclin A2+ cells (panel D), Cyclin A2– cells (G1 phase, panel E) in MP41 cells depleted of BAP1. Representative immunofluorescence images are shown in F. Red line: mean. *p < 0.05, **p < 0.01, ns: not significant. P-values by one-way ANOVA with Tukey's correction.

Figure 5. PTC-209 partially rescues NHEJ defects in BAP1-depleted cells.
(A) Representative immunofluorescence images of RPA (green) and Cyclin A2 (red) in BAP1-depleted MP41 cells ± PTC-209 treatment. DAPI stains DNA. Cells were treated with PTC-209 (0.1 µM, 48 h) prior to irradiation and collected at 3 h post-IR. Arrows mark Cyclin A2– (G1 phase) cells with RPA foci. Scale bar: 10 µm.
(B, C) Scatter dot plots showing (B) the percentage of RPA+ Cyclin A2– cells and (C) the number of RPA foci per Cyclin A2– cell at 3 h post-IR. Red line: mean. ****p < 0.0001, ***p < 0.001, **p < 0.01, ns: not significant. P-values by one-way ANOVA with Tukey's correction.
(D) Representative immunofluorescence images of 53BP1 (green) in BAP1-depleted MP41 cells ± PTC-209 treatment at 1 and 3 h post-IR. DAPI stains DNA. Scale bar: 10 µm.
(E) Scatter dot plot quantifying 53BP1 foci per cell. Red line: median. ****p < 0.0001, **p < 0.01, ns: not significant. P-values by one-way ANOVA with Tukey's correction.
(F) Schematic model. In BAP1-proficient cells, BAP1 deubiquitylates H2AK119ub deposited by PRC1, permitting 53BP1 recruitment and NHEJ execution in G1. In BAP1-depleted cells, H2AK119ub accumulates, blocking 53BP1 loading, and driving aberrant DNA end resection with RPA recruitment in G1, where HR is not available.

Supplementary Figure S1. BAP1 mutation status does not correlate with genomic instability in mesothelioma (MM), intrahepatic cholangiocarcinoma (ICC), and clear cell renal cell carcinoma (ccRCC).
(A) Kaplan–Meier survival curve for mesothelioma patients with BAP1 wild-type (green) or BAP1-mutated (red) tumors. P-values indicated. Data from TCGA GDC (via cBioPortal).
(B–D) Violin plots showing aneuploidy score, mutation count, fraction of genome altered, and microsatellite instability (MSI) score for BAP1 wild-type versus BAP1-mutated tumors in mesothelioma (B), ICC (C), and ccRCC (D). Red line: median. ns: not significant. P-values by unpaired t-test. Cohorts retrieved from TCGA PanCancer Atlas (mesothelioma, ccRCC), MSK Hepatology 2021 and MSK Clin Cancer Res 2021 (ICC).
(E) Western blot confirming BAP1 silencing efficiency in MP41 cells used for pan-nuclear γH2AX immunofluorescence assays (72 h post-siRNA).

Supplementary Figure S2. BAP1 depletion impairs RAD51 and 53BP1 recruitment after IR-induced DNA damage.
(A) Western blot confirming BAP1 and BRCA1 knockdown in MP41 cells used for RAD51/53BP1 immunofluorescence assays (72 h post-siRNA).
(B, E) Representative immunofluorescence images of RAD51 (red, B) and 53BP1 (green, E) in MP41 cells following BAP1 or BRCA1 depletion at the indicated hours post-IR (5 Gy). DAPI stains DNA. Scale bar: 10 µm.
(C, F) Scatter dot plots showing the number of RAD51 (C) or 53BP1 (F) foci per cell (dots) across two independent experiments. Red line: mean (C) or median (F). ****p < 0.0001, ***p < 0.001, **p < 0.01, *p < 0.05, ns: not significant. P-values by one-way ANOVA with Tukey's correction.
(D, G) Violin plots showing the percentage of RAD51+ cells (>2 foci/nucleus) (D) or 53BP1+ cells (>5 foci/nucleus) (G) over the total population per field (dots) in two independent experiments. Red

line: median. ****p < 0.0001, ***p < 0.001, **p < 0.01, *p < 0.05, ns: not significant. P-values by one-way ANOVA with Tukey's correction.

Supplementary Figure S3. BAP1 depletion impairs HR and SSA repair efficiency in HR-GFP/3′EGFP U2OS cells.
(A) Schematic of the integrated HR-EGFP/3′EGFP reporter construct in the selected U2OS clone.
(B) Western blot confirming BAP1 and BRCA1 knockdown at 72 h post-siRNA in U2OS HR-EGFP/3′EGFP cells.
(C) Bar plot showing HR/SSA repair efficiency across ≥3 independent experiments (dots). Data normalized to control and shown as mean ± SD. ****p < 0.0001. P-values by one-way ANOVA with Tukey's correction.
(D) Representative flow cytometry plots showing the percentage of RFP+ cells (yellow gate, top panels) transfected with I-SceI-RFP within the total population, and GFP+ cells within the RFP+ gate (bottom panels). RFP: Y585-PE-A; SSC: side scatter.

Supplementary Figure S4. I-SceI transfection efficiency in HR-GFP/5′EGFP and PIMEJ5GFP U2OS cells.
(A) Western blot confirming BAP1 and BRCA1 knockdown at 72 h post-siRNA in U2OS HR-GFP/5′EGFP cells
(B) Real-time PCR confirming BAP1 knockdown in U2OS PIMEJ5GFP cells at 72 h post-siRNA (top). (C) Flow cytometry plots showing RFP+ populations (yellow gate) after I-SceI-RFP transfection upon BAP1 depletion (bottom).
(D) Representative flow cytometry plots showing the proportion of RFP+ cells (yellow gate) following I-SceI-RFP transfection upon BAP1 or BRCA1 depletion (upper right and lower panels). RFP: Y585-PE-A; SSC: side scatter.

Supplementary Figure S5. PTC-209 treatment modulates DSB repair defects in BAP1-depleted cells.
(A) Cell cycle analysis on synchronised MP41 showing the fraction of phase G1, S and G2 cells. Cells were collected at 6 hours post Nocodazole release.
(B) Western blot confirming BAP1 and BRCA1 knockdown in MP41 cells used for Cyclin A2/RPA staining experiment in Figure 4.
(C) Western blot confirming BAP1 knockdown in MP41 cells treated with PTC-209 in the experiment in Figure 4.
(D) Bar plot showing the percentage of Cyclin A2+ and Cyclin A2– cells under the indicated conditions (non-irradiated and 3 h post-IR) in control and BAP1-depleted MP41 cells. Data are mean ± SD from 2 independent experiments.

FIGURE1

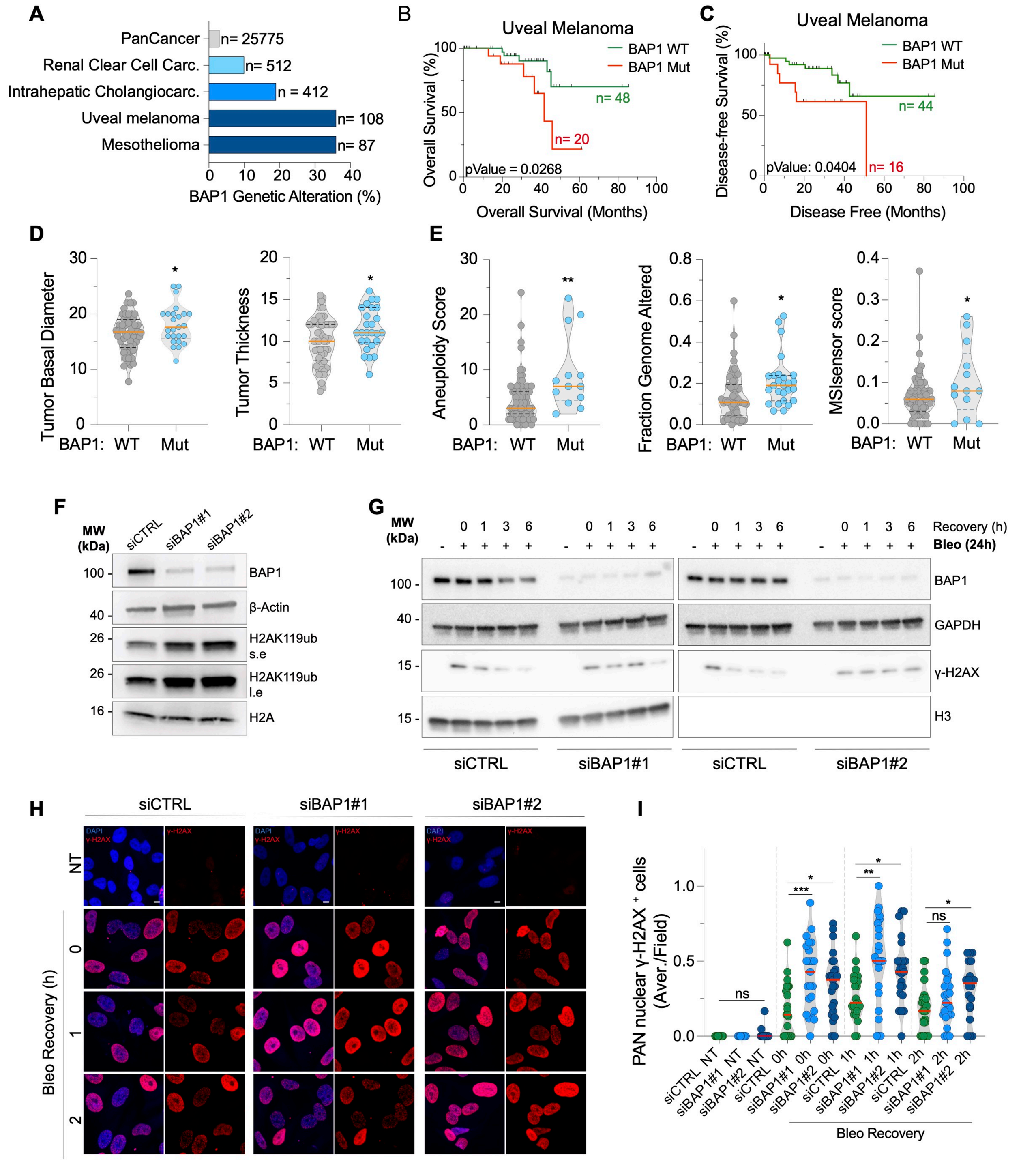
A
PanCancer
n= 25775
Renal Clear Cell Carc.
n= 512
Intrahepatic Cholangiocarc.
n = 412
Uveal melanoma
n= 108
Mesothelioma
n= 87
BAP1 Genetic Alteration (%)
B
Uveal Melanoma
BAP1 WT
BAP1 Mut
n= 48
n= 20
pValue = 0.0268
Overall Survival (%)
Overall Survival (Months)
C
Uveal Melanoma
BAP1 WT
BAP1 Mut
n= 44
n= 16
pValue: 0.0404
Disease-free Survival (%)
Disease Free (Months)
D
Tumor Basal Diameter
Tumor Thickness
E
Aneuploidy Score
Fraction Genome Altered
MSIsensor score
BAP1: WT Mut
F
MW (kDa)
siCTRL
siBAP1#1
siBAP1#2
BAP1
β-Actin
H2AK119ub s.e
H2AK119ub l.e
H2A
G
MW (kDa)
Recovery (h)
Bleo (24h)
BAP1
GAPDH
γ-H2AX
H3
siCTRL
siBAP1#1
siBAP1#2
H
siCTRL
siBAP1#1
siBAP1#2
DAPI
γ-H2AX
NT
Bleo Recovery (h)
I
PAN nuclear γ-H2AX + cells (Aver./Field)
ns
siCTRL NT
siBAP1#1 NT
siBAP1#2 NT
siCTRL 0h
siBAP1#1 0h
siBAP1#2 0h
siCTRL 1h
siBAP1#1 1h
siBAP1#2 1h
siCTRL 2h
siBAP1#1 2h
siBAP1#2 2h
Bleo Recovery

FIGURE 2

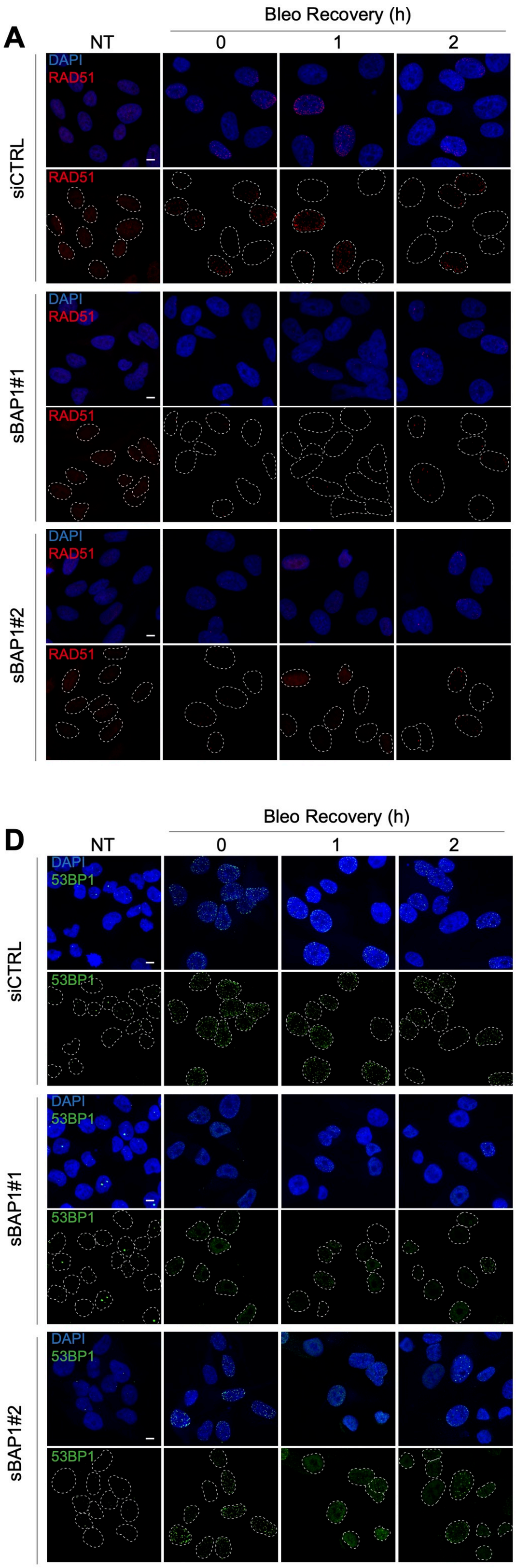
A
Bleo Recovery (h)
NT
0
1
2
siCTRL
sBAP1#1
sBAP1#2
DAPI
RAD51
D
53BP1

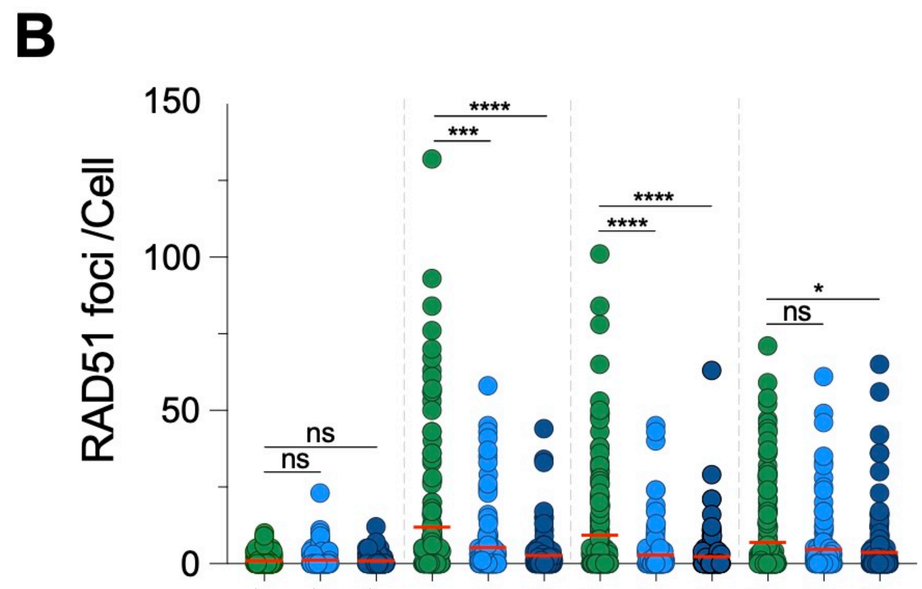
B
RAD51 foci /Cell
150
100
50
0
ns
****
***
*
siCTRL nt
siBAP1#1 nt
siBAP1#2 nt
siCTRL 0h
siBAP1#1 0h
siBAP1#2 0h
siCTRL 1h
siBAP1#1 1h
siBAP1#2 1h
siCTRL 2h
siBAP1#1 2h
siBAP1#2 2h
Bleo Recovery

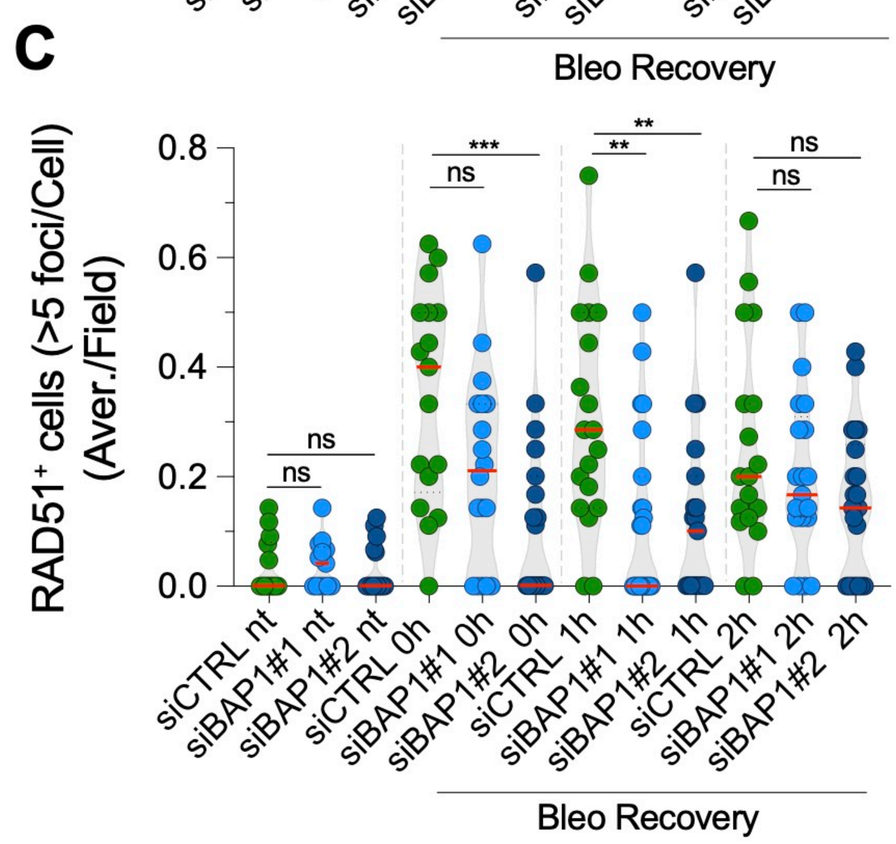
C
RAD51+ cells (>5 foci/Cell)
(Aver./Field)
0.8
0.6
0.4
0.2
0.0
ns
***
**
siCTRL nt
siBAP1#1 nt
siBAP1#2 nt
siCTRL 0h
siBAP1#1 0h
siBAP1#2 0h
siCTRL 1h
siBAP1#1 1h
siBAP1#2 1h
siCTRL 2h
siBAP1#1 2h
siBAP1#2 2h
Bleo Recovery

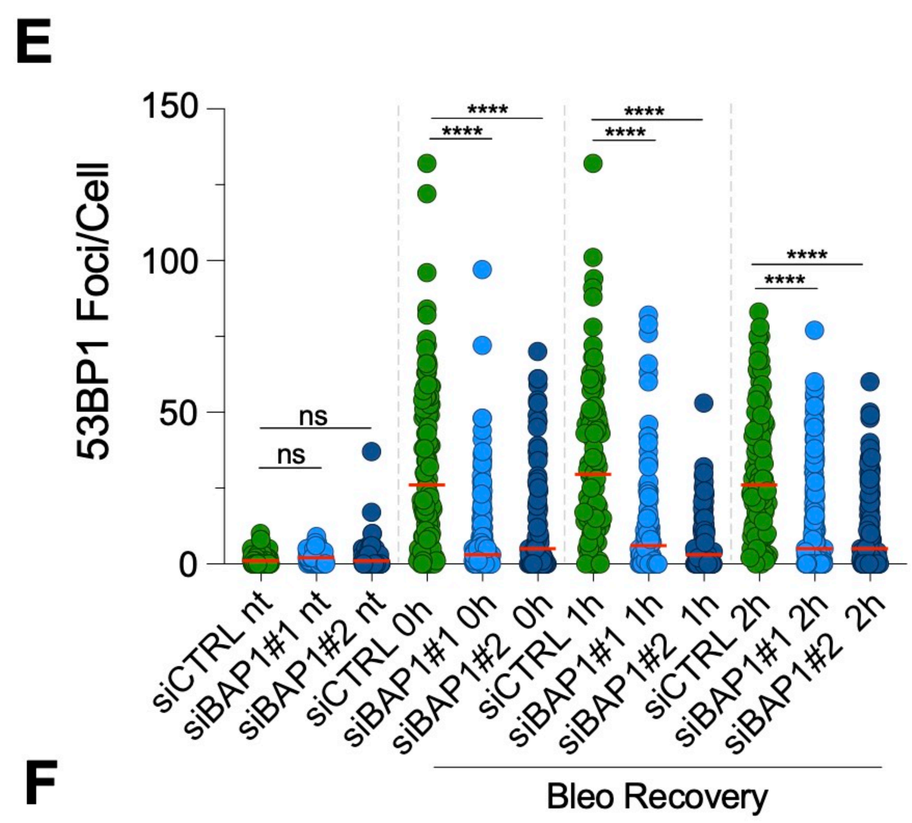
E
53BP1 Foci/Cell
150
100
50
0
ns
****
siCTRL nt
siBAP1#1 nt
siBAP1#2 nt
siCTRL 0h
siBAP1#1 0h
siBAP1#2 0h
siCTRL 1h
siBAP1#1 1h
siBAP1#2 1h
siCTRL 2h
siBAP1#1 2h
siBAP1#2 2h
Bleo Recovery

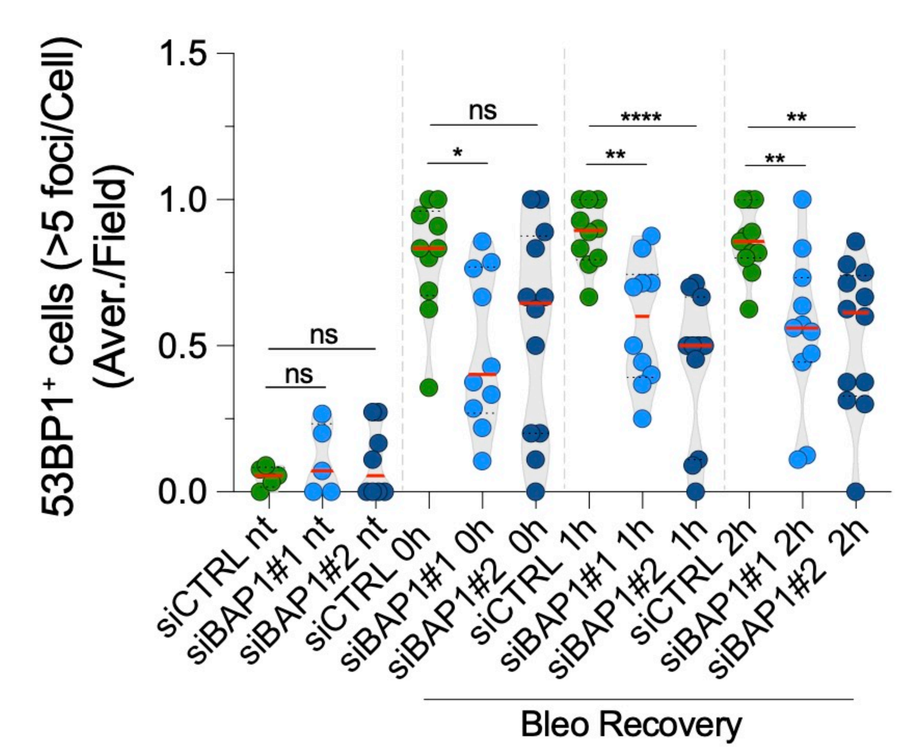
F
53BP1+ cells (>5 foci/Cell)
(Aver./Field)
1.5
1.0
0.5
0.0
ns
*
**
****
siCTRL nt
siBAP1#1 nt
siBAP1#2 nt
siCTRL 0h
siBAP1#1 0h
siBAP1#2 0h
siCTRL 1h
siBAP1#1 1h
siBAP1#2 1h
siCTRL 2h
siBAP1#1 2h
siBAP1#2 2h
Bleo Recovery

FIGURE3

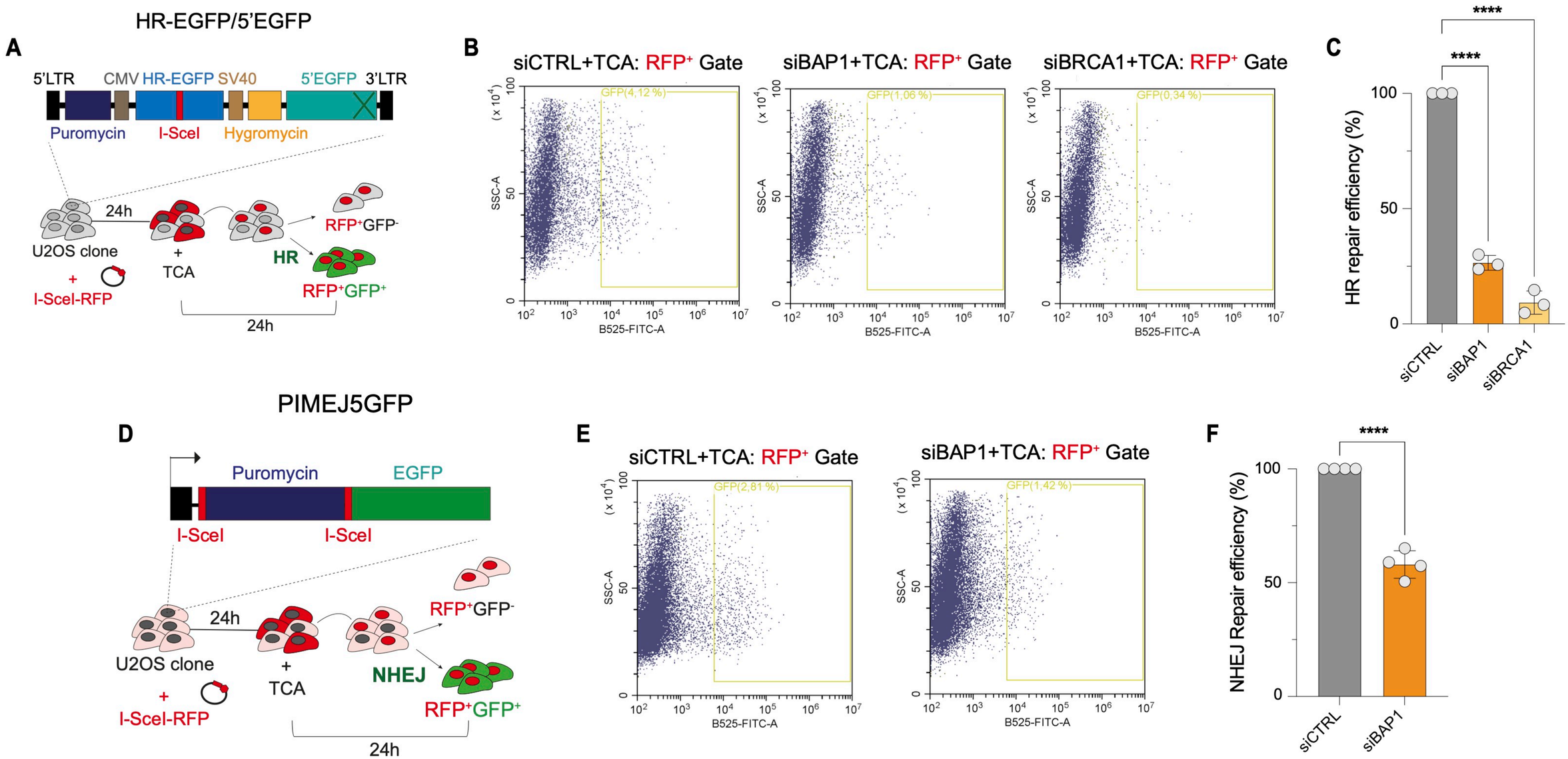
A
HR-EGFP/5'EGFP
5'LTR
CMV
HR-EGFP
SV40
5'EGFP
3'LTR
Puromycin
I-SceI
Hygromycin
24h
U2OS clone
+
I-SceI-RFP
+
TCA
HR
RFP+GFP-
RFP+GFP+
24h
B
siCTRL+TCA: RFP+ Gate
siBAP1+TCA: RFP+ Gate
siBRCA1+TCA: RFP+ Gate
GFP(4,12 %)
GFP(1,06 %)
GFP(0,34 %)
SSC-A
B525-FITC-A
C
HR repair efficiency (%)
****
****
siCTRL
siBAP1
siBRCA1
PIMEJ5GFP
D
Puromycin
EGFP
I-SceI
I-SceI
24h
U2OS clone
+
I-SceI-RFP
+
TCA
NHEJ
RFP+GFP-
RFP+GFP+
24h
E
siCTRL+TCA: RFP+ Gate
siBAP1+TCA: RFP+ Gate
GFP(2,81 %)
GFP(1,42 %)
SSC-A
B525-FITC-A
F
NHEJ Repair efficiency (%)
****
siCTRL
siBAP1

FIGURE 4

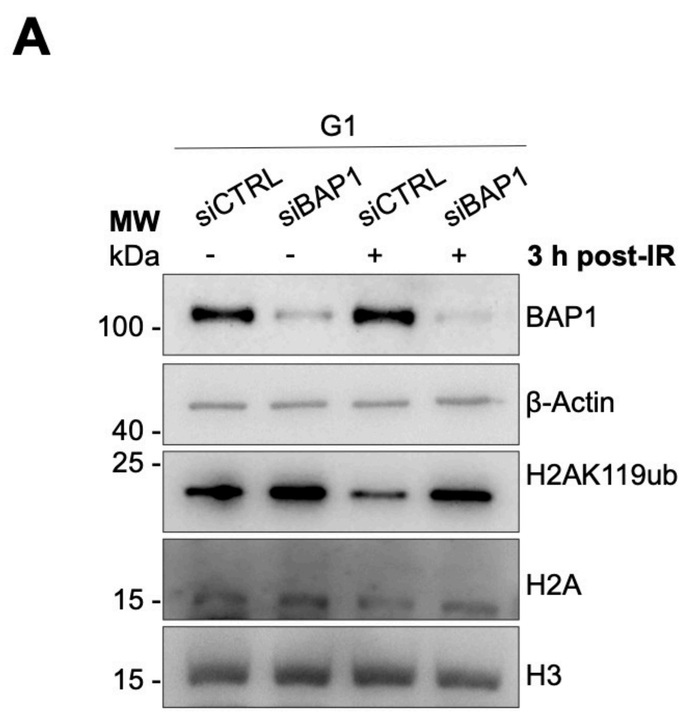
A
G1
siCTRL
siBAP1
siCTRL
siBAP1
MW
kDa
- - + +
3 h post-IR
100
BAP1
β-Actin
40
25
H2AK119ub
15
H2A
15
H3

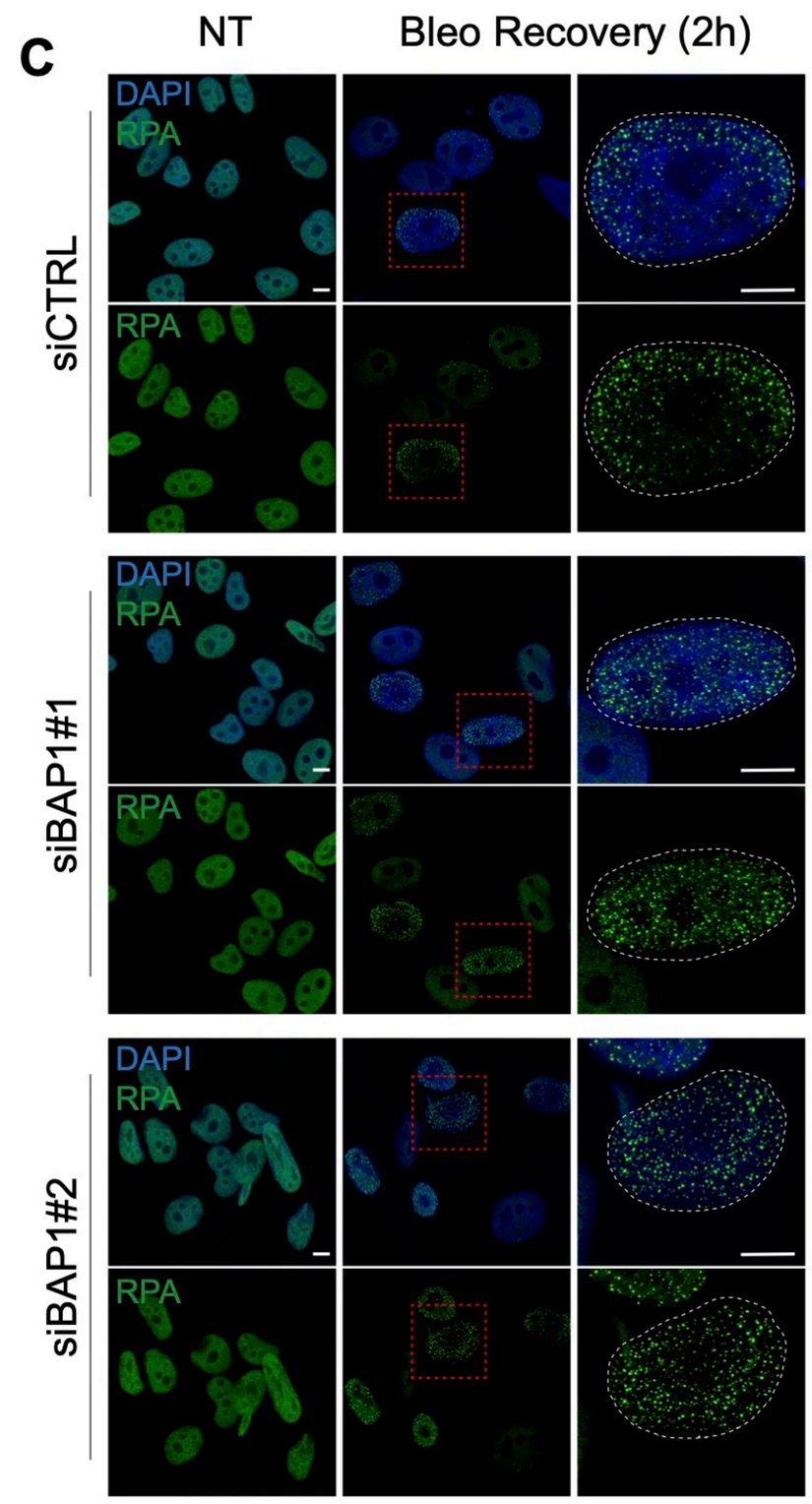
C
NT
Bleo Recovery (2h)
siCTRL
siBAP1#1
siBAP1#2
DAPI
RPA

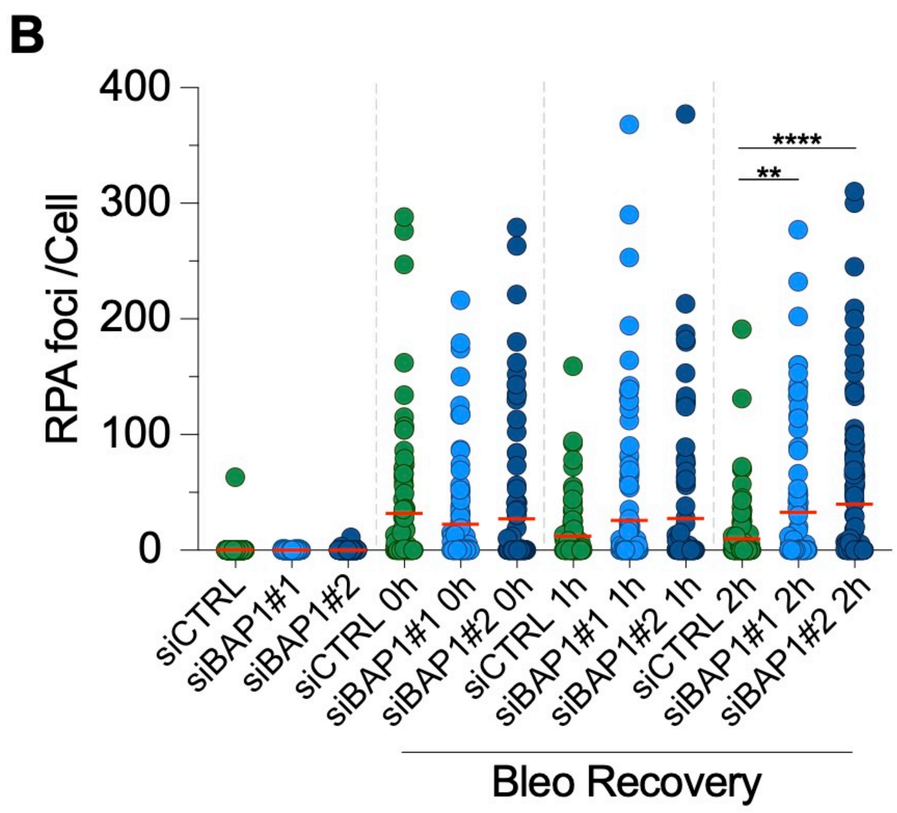
B
RPA foci /Cell
400
300
200
100
0
****
**
siCTRL
siBAP1#1
siBAP1#2
siCTRL 0h
siBAP1#1 0h
siBAP1#2 0h
siCTRL 1h
siBAP1#1 1h
siBAP1#2 1h
siCTRL 2h
siBAP1#1 2h
siBAP1#2 2h
Bleo Recovery

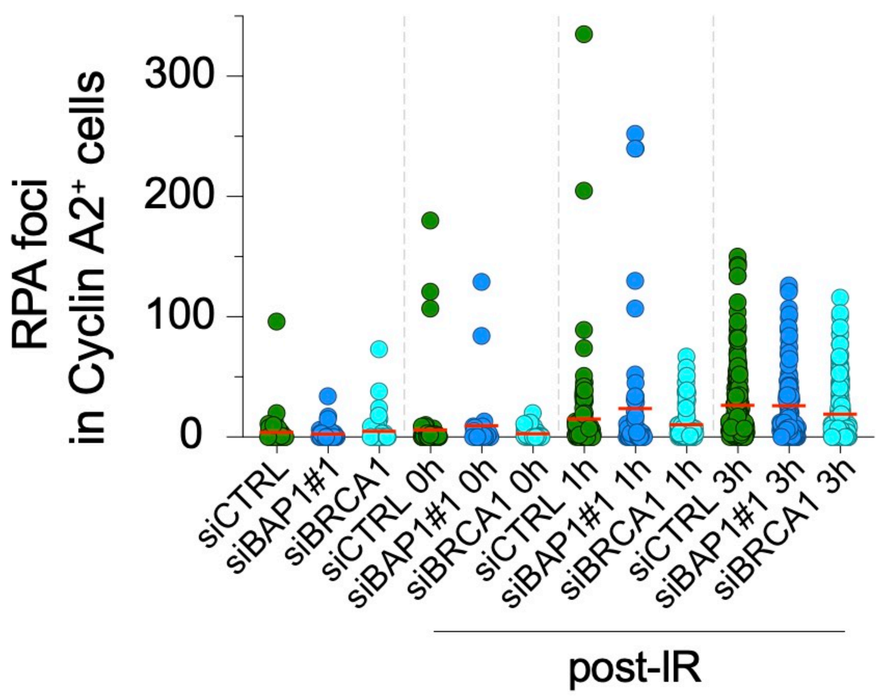
D
RPA foci
in Cyclin A2+ cells
300
200
100
0
siCTRL
siBAP1#1
siBRCA1
siCTRL 0h
siBAP1#1 0h
siBRCA1 0h
siCTRL 1h
siBAP1#1 1h
siBRCA1 1h
siCTRL 3h
siBAP1#1 3h
siBRCA1 3h
post-IR

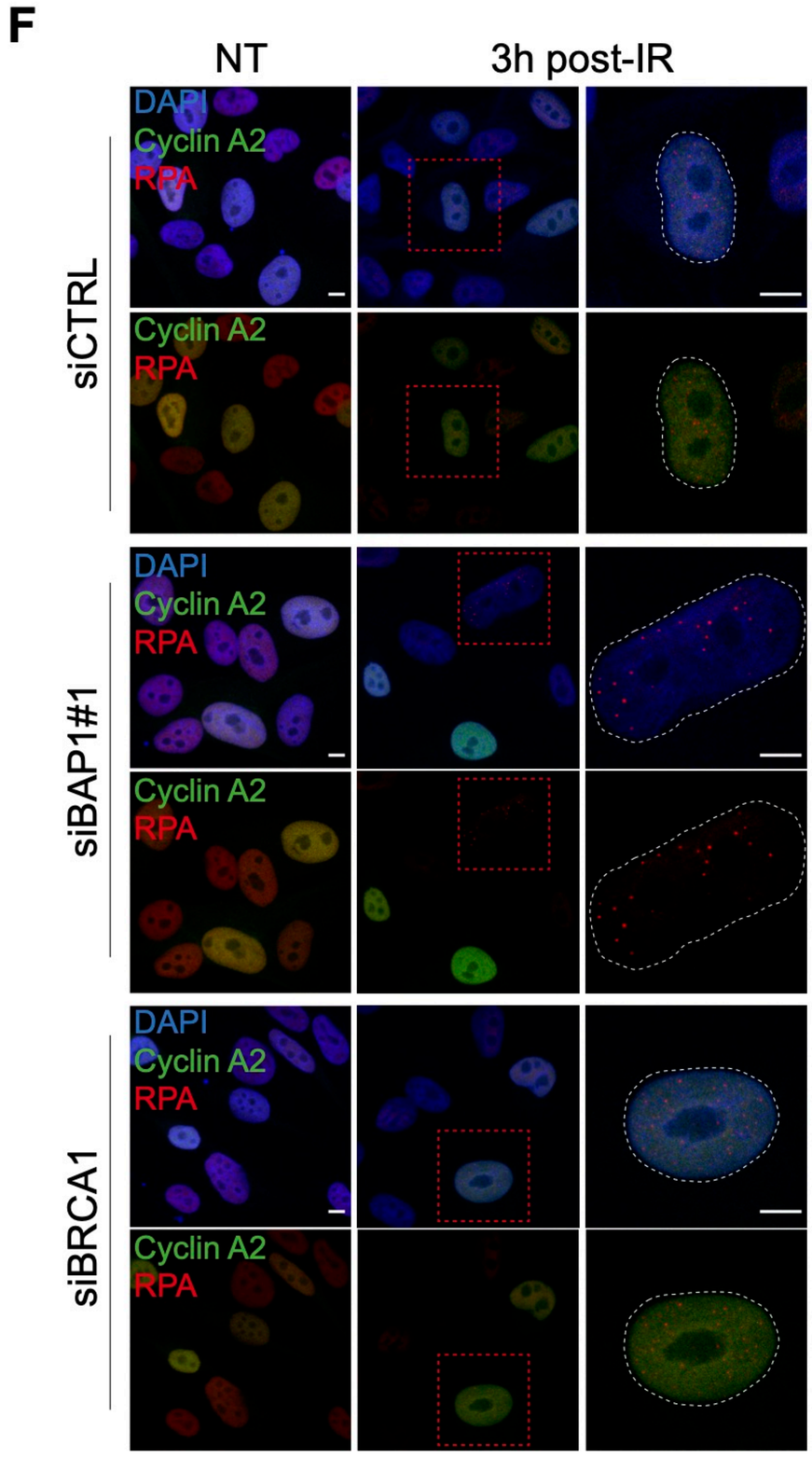
F
NT
3h post-IR
siCTRL
siBAP1#1
siBRCA1
DAPI
Cyclin A2
RPA

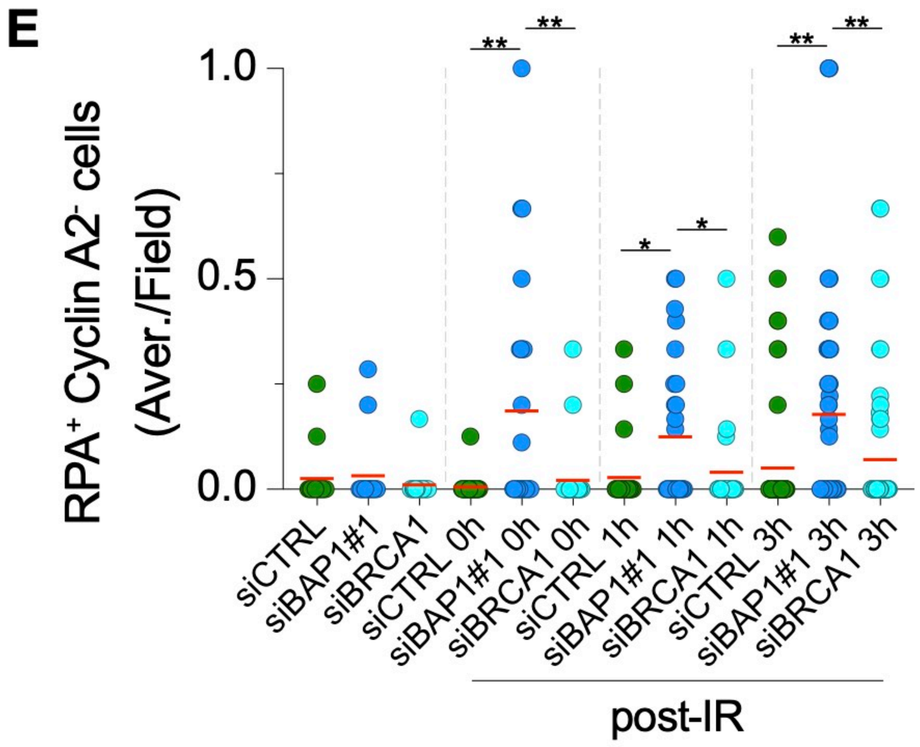
E
RPA+ Cyclin A2- cells
(Aver./Field)
1.0
0.5
0.0
**
**
*
*
**
**
siCTRL
siBAP1#1
siBRCA1
siCTRL 0h
siBAP1#1 0h
siBRCA1 0h
siCTRL 1h
siBAP1#1 1h
siBRCA1 1h
siCTRL 3h
siBAP1#1 3h
siBRCA1 3h
post-IR

FIGURE 5

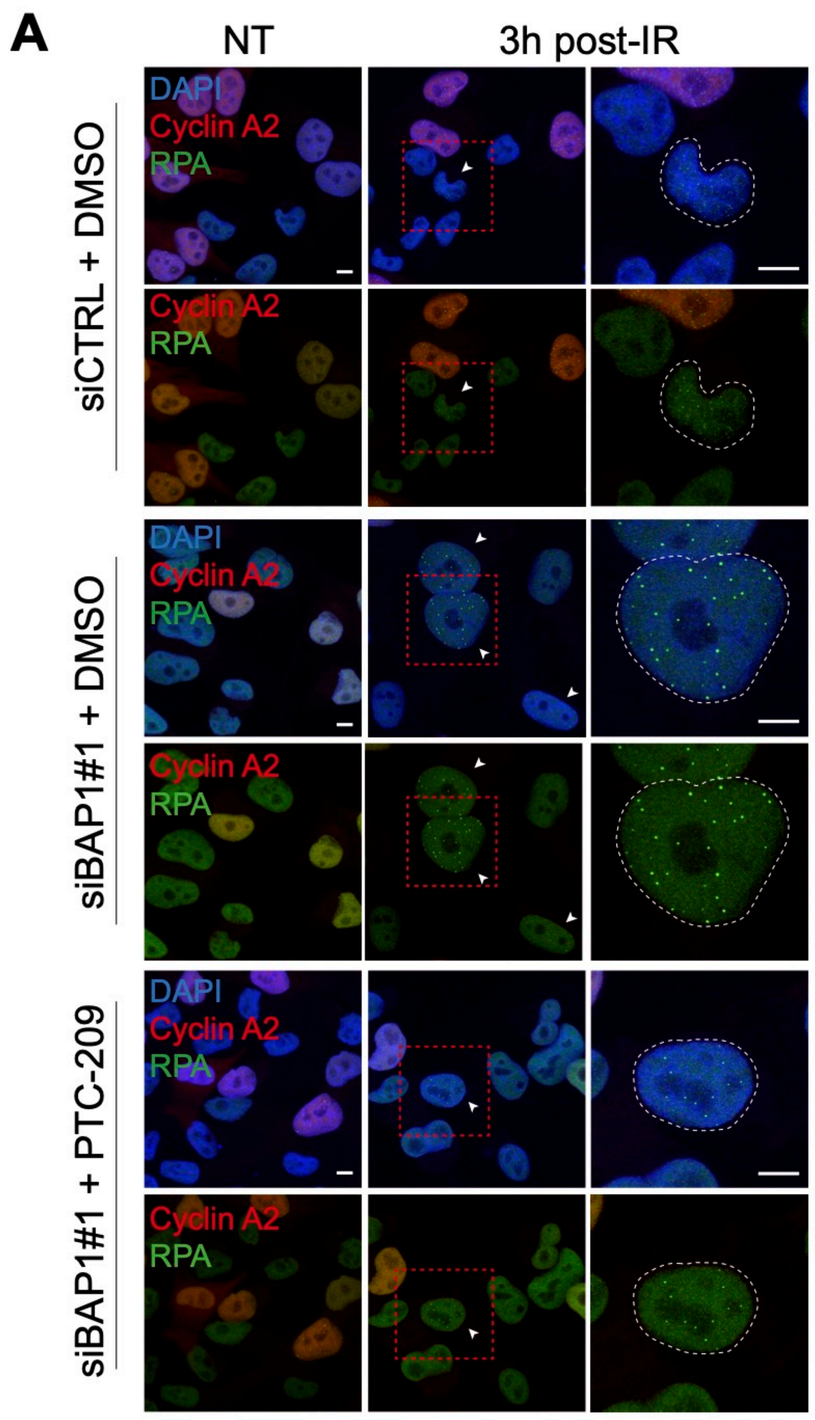
A
NT
3h post-IR
siCTRL + DMSO
siBAP1#1 + DMSO
siBAP1#1 + PTC-209
DAPI
Cyclin A2
RPA

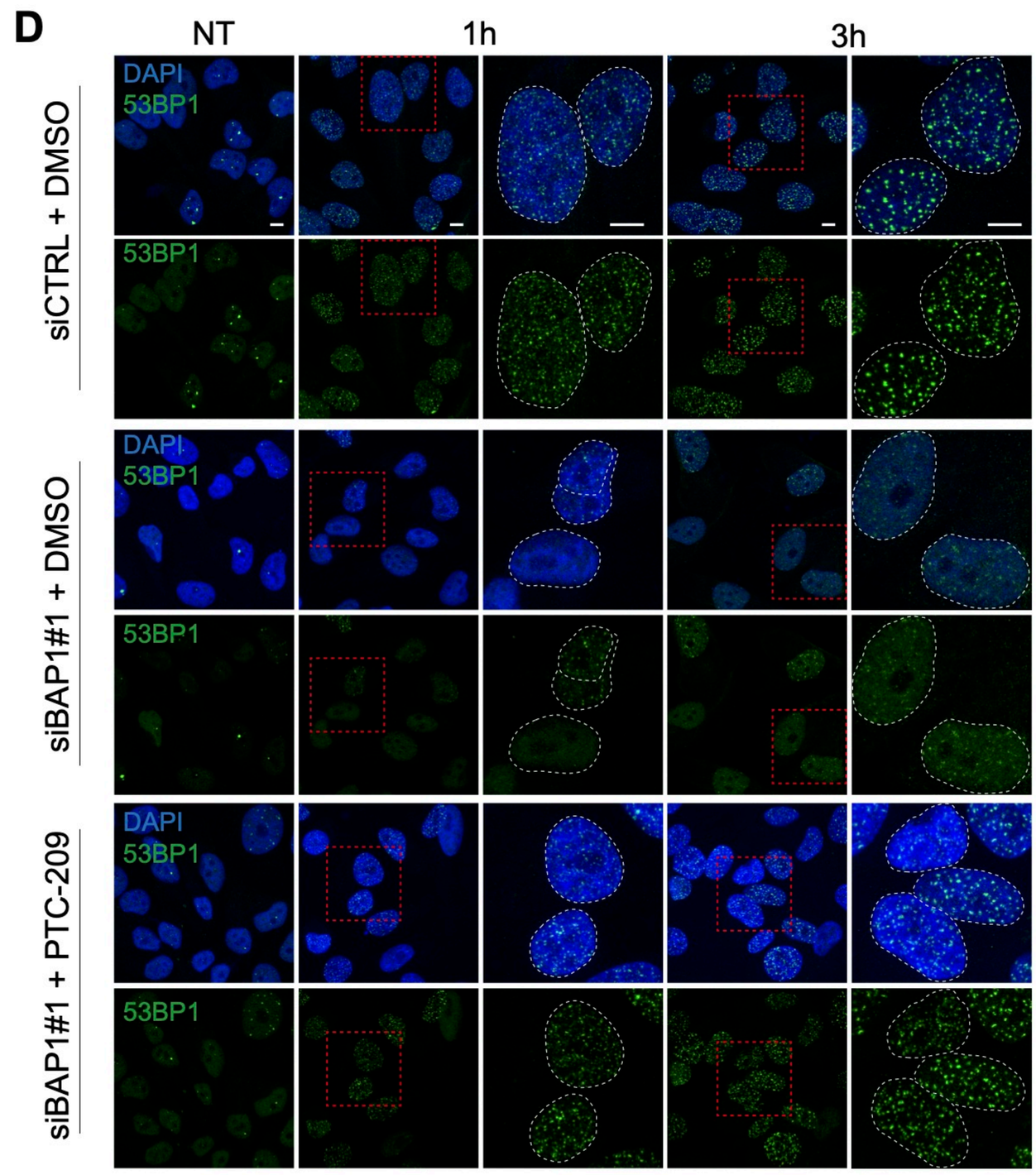
D
post-IR
NT
1h
3h
siCTRL + DMSO
siBAP1#1 + DMSO
siBAP1#1 + PTC-209
DAPI
53BP1

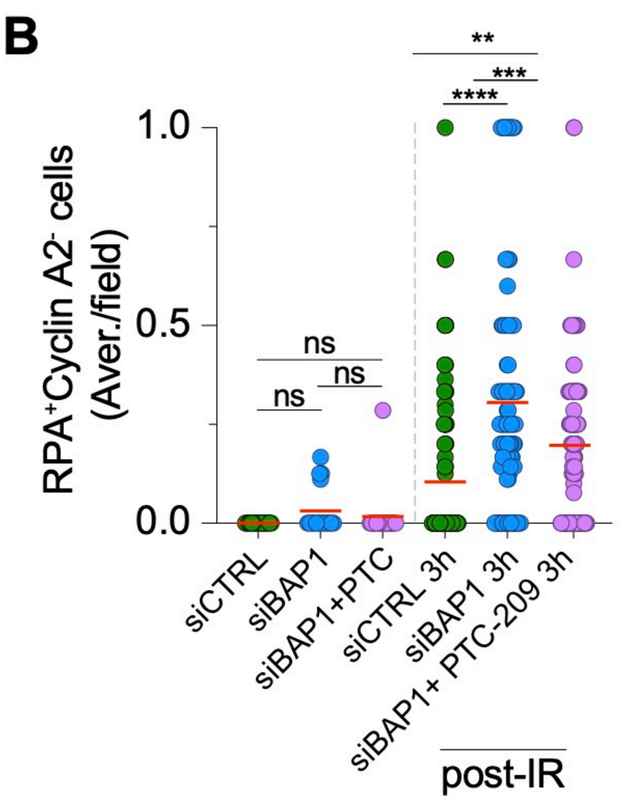
B
RPA+Cyclin A2- cells (Aver./field)
1.0
0.5
0.0
ns
ns
ns
**
***
****
siCTRL
siBAP1
siBAP1+PTC
siCTRL 3h
siBAP1 3h
siBAP1+ PTC-209 3h
post-IR

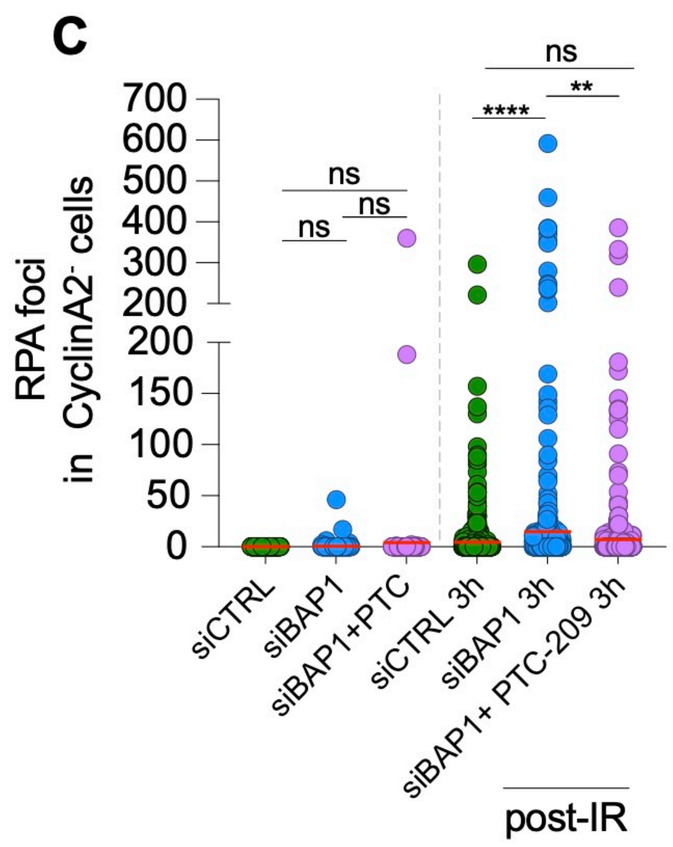
C
RPA foci in CyclinA2- cells
700
600
500
400
300
200
200
150
100
50
0
ns
ns
ns
****
**
siCTRL
siBAP1
siBAP1+PTC
siCTRL 3h
siBAP1 3h
siBAP1+ PTC-209 3h
post-IR

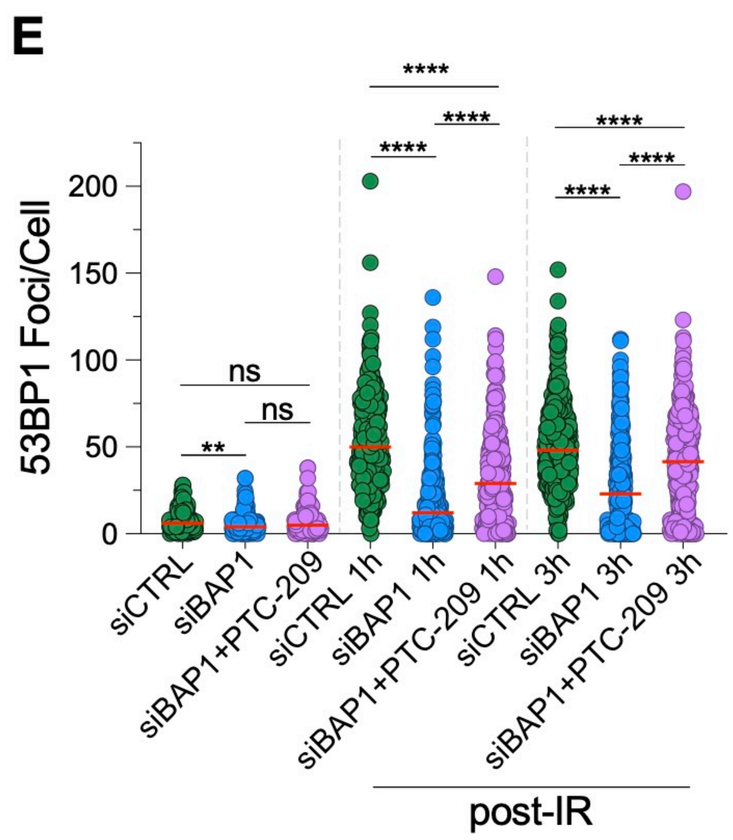
E
53BP1 Foci/Cell
200
150
100
50
0
ns
ns
**
****
****
****
****
****
****
siCTRL
siBAP1
siBAP1+PTC-209
siCTRL 1h
siBAP1 1h
siBAP1+PTC-209 1h
siCTRL 3h
siBAP1 3h
siBAP1+PTC-209 3h
post-IR

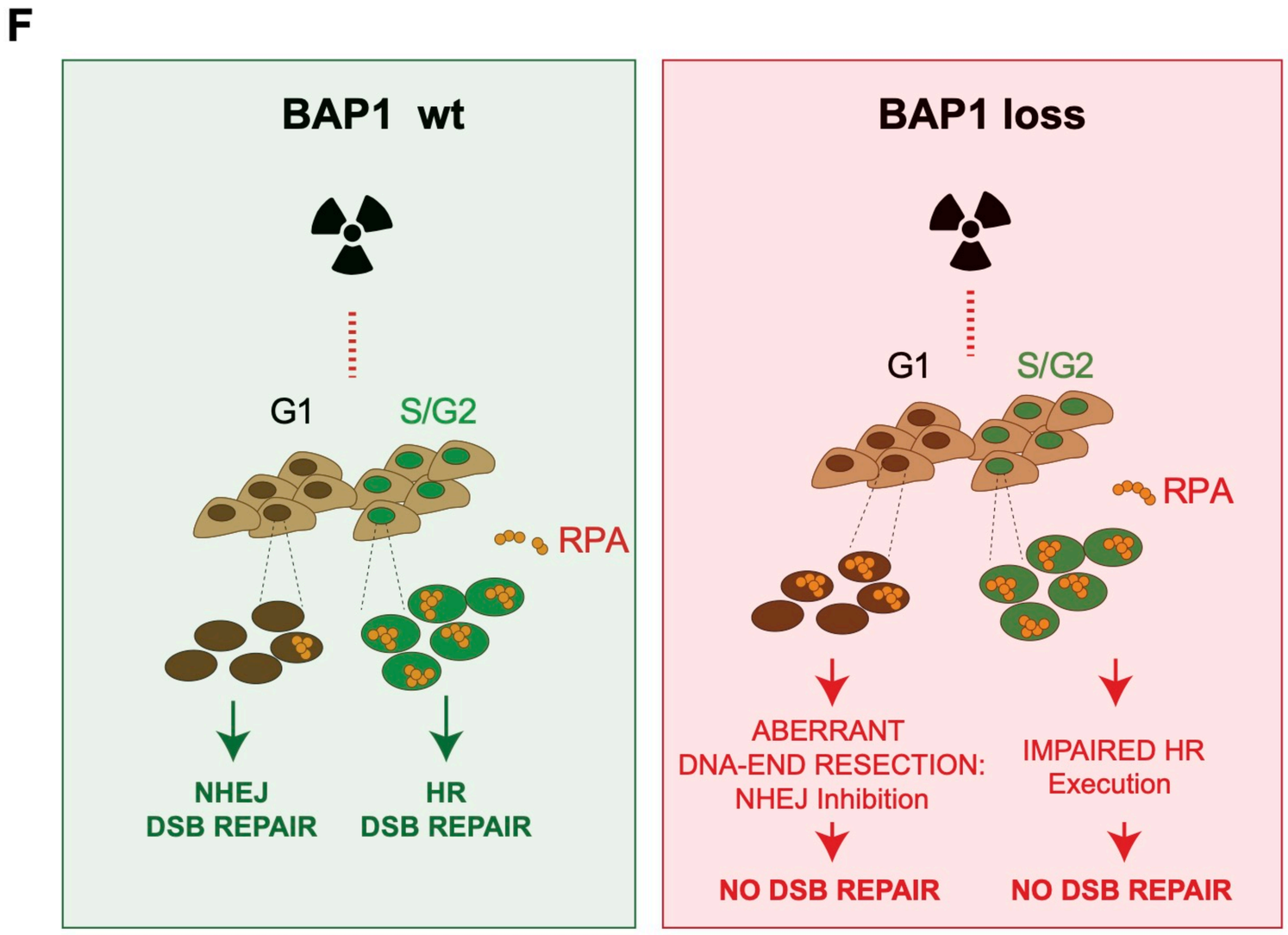
F
BAP1 wt
G1
S/G2
RPA
NHEJ
DSB REPAIR
HR
DSB REPAIR
BAP1 loss
G1
S/G2
RPA
ABERRANT
DNA-END RESECTION:
NHEJ Inhibition
IMPAIRED HR
Execution
NO DSB REPAIR
NO DSB REPAIR